MOLECULAR DYNAMIC SIMULATIONS OF RAFT FORMATION AND FULLERENE TRANSPORT IN LIPID MEMBRANES

By

TARUN NARRA

A THESIS PRESENTED TO THE GRADUATE SCHOOL
OF THE UNIVERSITY OF FLORIDA IN PARTIAL FULFILLMENT
OF THE REQUIREMENTS FOR THE DEGREE OF
MASTER OF SCIENCE

UNIVERSITY OF FLORIDA

2013

To my mom, dad and sister

ACKNOWLEDGMENTS

I sincerely thank my research advisor Prof. Dmitry Kopelevich for his constant support and encouragement throughout my research work. His guidance enabled me to develop an understanding of molecular dynamics simulation. His valuable inputs brought in great value to this work. I thank Prof. Anuj Chuahan for his suggestions.

I thank Dr.Yong Nam Ahn of our research group for his help and suggestions during my research which helped me to learn the simulation software.

TABLE OF CONTENTS

page

LIST OF TABLES

LIST OF FIGURES

Abstract of Thesis Presented to the Graduate School
of the University of Florida in Partial Fulfillment of the
Requirements for the Degree of Master of Science

MOLECULAR DYNAMIC SIMULATIONS OF RAFT FORMATION AND FULLERENE TRANSPORT IN LIPID MEMBRANES

By

Tarun Narra

May 2013

Chair: Dmitry I,Kopelevich
Major: Chemical Engineering

Cell membranes are known to contain many types of lipids which can form domains resulting in lateral structural heterogeneity. The lipid domains which are tightly packed and more ordered than their surroundings are called rafts. Understanding the aggregation of lipids into rafts is crucial in biological applications. In this study we have used coarse grained molecular dynamic simulations to explore two mechanisms of raft formations, namely ion crossbridging and cholesterol induced raft formation. For exploring the former, we considered an anionic surfactant, a neutral surfactant and artificial lipids with varying number of charges. We observed that the tendency towards the aggregate formation is determined by the number of charged beads in lipid head groups. Specifically, artificial lipids with three negatively charged beads in the head groups aggregate due to calcium ion cross bridging. On the other hand, the surfactants and lipids which have only one charged head group bead did not show aggregation. The other mechanism was explored using ternary mixture of cholesterol, saturated and unsaturated lipids which is known to form liquid ordered(L_o) and liquid disordered(L_d) phases. We also investigated effects of the membrane composition and structure on

transport across the membranes. To this end, free energy profiles of the transport of model hydrophobic fullerene nanoparticle across the L_o and L_d phases were reported. Our results show that fullerene encounters a large energy barrier while entering the L_o phase due to tight packing of lipids and cholesterol. No significant energy barrier was observed for transport into the L_d phase.

CHAPTER 1
INTRODUCTION

1.1 Background

Biological cell membranes are lipid bilayers embedded with proteins. They serve several functions, including protecting the cell interior from its environment and controlling transport of molecules in and out of the cell. These membranes are known to contain many types of lipids which can form domains resulting in lateral structural heterogeneity. The lipid domains which are tightly packed and more ordered than their surroundings are called rafts. The mechanism of the raft formation is still not completely understood. Earlier studies have proposed several mechanisms including electrostatic coupling (1), interfacial energy minimizations (2), lipid and cholesterol interactions (3) and composition curvature coupling (4) for explaining the heterogeneity. The main focus of this thesis is to apply molecular dynamic (MD) simulations to investigate two of the mechanisms of the raft formations in a lipid bilayer namely by ion crosslinking and by cholesterol.

The first part of the thesis studies the interaction of surfactants in membrane. Surfactants are amphiphilic molecules containing hydrophilic head groups and hydrophobic tail groups. Interactions between the surfactants and the lipid bilayers have been extensively studied due to their importance in drug delivery and food industry. Previous studies have shown that contact of surfactants with a lipid membrane may result in increase of the membrane permeability (5)(6). This increase in permeability is often transient (7), i.e. the permeability of lipid bilayer eventually decreases healing the bilayer. A possible mechanism for the healing may be due to aggregation of surfactants

in the membrane (8). Therefore we have explored the likeliness of aggregation surfactants in a membrane using MD simulations.

In the first set of simulation studies, we have explored the raft formations in lipid membranes due to the crossbridging by ions. This study was conducted to understand the influence of ions in stabilizing the rafts.

The presence of cholesterol at biologically relevant concentrations (10-30%) in a lipid membrane consisting of saturated and unsaturated lipids results in the raft formation. In the next set of simulations we have explored the lipid segregation which occurred due to the presence of cholesterol in a ternary lipid membrane.

In addition we have explored the transport of nanoparticle across the different phases formed in ternary mixture of saturated, unsaturated lipids and cholesterol. The nanoparticles are ultrafine particles that have size in the order of one billionth of a meter. These particles exhibit different size-dependent physical and chemical properties from those of their bulk counterparts. Research on nanoparticles has revolutionized various areas of science and technology. They have various applications in such fields as medicine, electronics, food packaging, paints, materials, cosmetics and fabrics. Currently more than a thousand commercial products containing nanoparticles are available on the market and more products are being added almost every week according to Woodrow Wilson Centre's Project on Emerging Nanotechnologies (9). Due to this rapid increase in number of products containing nanoparticles, it is evident that humans and the environment are coming into contact with the manufactured nanoparticles (MNs) either by accident or by intention. It is therefore important to

analyze the possibility of any unintended consequences of these particles on humans and their environment.

1.2 Thesis Outline

The thesis is organized as follows:

In Chapter 2, the methods of molecular dynamic (MD) simulations are presented. The coarse gained molecular models which are used for extending the time and length scales accessible to the simulation are discussed. Constrained simulations employed in analysis of the fullerene transport are also described.

In Chapter 3, analysis of stability of pre-assembled surfactant aggregates is presented. Then the simulations which aimed at understanding the aggregations of the lipids due to crossbridging by calcium ions are presented. Next we report our simulations of domain formation in a mixture containing cholesterol and saturated and unsaturated lipids.

In Chapter 4, the model and simulation details of transport of the fullerene nanoparticle across lipid membrane domains is presented and analyzed.

CHAPTER 2
METHODS

2.1 Molecular Dynamics Simulations

Molecular dynamic (MD) simulations have become one of the principal tools for providing detailed information on nanoscale systems. This information in general cannot be easily obtained through macroscopic experiments due to the small time and length scales of the processes. They also act as a complementary tool for verifying experimental results or to test theoretical predictions.

MD simulations use Newton's equations of motion to analyze dynamic behavior of microscopic systems. The forces (F_i) acting on the particle *i* of mass m_i will move it to new positions by solving

$$F_i = m_i \frac{\partial^2 r_i}{\partial t^2} \tag{2.1}$$

Where F_i is the negative partial derivative of the potential function $V(r_1, r_2 \ldots . r_N)$, with respect to the particle position(r_i).

$$F_i = -\frac{\partial V(r)}{\partial r_i} \tag{2.2}$$

In our MD simulations we have used Verlet leap frog algorithm (10) for obtaining the evolution of coordinates and velocities of the particles. The leap frog algorithm uses the particle positions r_i at time *t* and velocities v_i at time $t - \frac{1}{2}\Delta t$ to compute the positions and velocities at next timestep

$$v_i(t+\frac{1}{2}\Delta t) = v_i(t-\frac{1}{2}\Delta t) + \frac{\Delta t}{m_i} F_i(t) \tag{2.3}$$

$$r_i(t+\Delta t) = r_i(t) + \Delta t v_i(t+\frac{1}{2}\Delta t) \tag{2.4}$$

For MD simulations, we need the initial positions and velocities of all the particles present in the system. The velocities of particles are generated from the Maxwell velocity distribution.

$$f_v(v_x, v_y, v_z) = \left(\frac{m}{2\pi kT}\right)^{3/2} \exp\left[\frac{-m(v_x^2 + v_y^2 + v_z^2)}{2kT}\right] \quad (2.5)$$

Here f_v is probability density of velocity, k is Boltzmann constant, T is temperature and v_x, v_y, v_z are the velocity components .

The particles that are to be simulated are usually contained in a rectangular box. Edge effects in a finite system are reduced by periodic boundary conditions (PBC). The PBC ensure that a molecule leaving from one side of the box re-enters the box on the opposite side.

Any simulation study typically consists of three steps. The first step is energy minimization. Two MD simulation runs are then carried out. The first MD simulation run known as equilibration run, uses strong temperature and/or pressure coupling for relaxing the system and to stabilize desired ensemble (NVT, NPT, etc.) properties. A production MD simulation is then carried out using weak temperature and/or pressure coupling. The data collected from the production MD simulation is used in the analysis.

2.1.1 Energy Minimization

If the initial positions of the particles contain overlapping atoms, MD simulations will fail due to very large forces. These forces need to be minimized before we perform MD simulations. In the current work we have used the steepest descent method for minimizing energy of our initial systems. The steepest descent is a quick and simple method to reduce the energy of the system. However its convergence near the local minimum can be very slow.

The steepest descent algorithm takes a step in the direction of the force. These steps move the system downhill along the potential energy landscape.

$$r_{n+1} = r_n + \frac{F_n}{\max\left(\left|F_n\right|\right)} h_n \tag{2.6}$$

Here vector r represents a vector of all 3*N* coordinates. F_n is the force and h_n is maximum displacement. If the (n+1)th step decreases the potential energy(i.e., $V_{n+1} < V_n$), the new positions are accepted and the displacement magnitude is increased, $h_{n+1} = 1.2h_n$. Otherwise the new positions are rejected and the displacement magnitude is decreased, $h_n = 0.2h_n$.

2.1.2 Temperature Coupling

All our simulations are performed in the NPT ensemble. To simulate constant temperatures in the simulations we have employed Berendsen temperature coupling scheme (11) in the equilibration MD run and Nose-Hoover temperature coupling scheme (12,13) in the production MD run.

2.1.2.1 Berendsen temperature coupling

The Berendsen algorithm is a strong coupling to a heat bath at a constant temperature T_0. The temperature deviations from the value of T_0 are corrected using

$$\frac{dT}{dt} = \frac{T_0 - T}{\tau} \tag{2.7}$$

The relaxation time τ is

$$\tau = \frac{2C_V \tau_T}{N_F k} \tag{2.8}$$

Here C_V represents heat capacity of the system, N_F is number of degrees of freedom and τ_T is temperature coupling time constant that we specify.

For maintaining the constant temperature, heat flow in or out of the system is controlled by scaling the velocities of each particle with a time-dependent factor λ after sufficient number of time steps n_{TC}. λ is given as

$$\lambda = \left[1 + \frac{n_{TC}\Delta t}{\tau_T} \left\{ \frac{T_0}{T(t - \frac{1}{2}\Delta t)} - 1 \right\} \right]^{1/2} \tag{2.9}$$

This algorithm however fails to generate good canonical ensemble as it suppresses the fluctuations of kinetic energy. It generates errors which scale with 1/number of particles in the systems. However, this algorithm is extremely efficient for relaxing the system to a target temperature. Hence this algorithm is used for the equilibration stage of our simulations.

2.1.2.2 Nose-Hoover temperature coupling

This coupling scheme was first proposed by Nose and later modified by Hoover. The Hamiltonian of the system is extended by using an additional degree of freedom for representing the thermal bath. The algorithm uses the following equations of motion for the particles:

$$\frac{d^2 r_i}{dt^2} = \frac{F_i}{m_i} - \frac{p_\xi}{Q}\frac{dr_i}{dt} \tag{2.10}$$

The equation of motion for the heat bath degree of freedom ξ is

$$\frac{dp_\xi}{dt} = \left(T - T_0\right) \tag{2.11}$$

Here p_ξ is the momentum corresponding to ξ, Q is known as the mass parameter of the thermal bath given by:

$$Q = \frac{\tau_T^2 T_o}{4\pi^2} \tag{2.12}$$

Here τ_T is chosen to be 4-5 times larger than relaxation time τ .

2.1.3 Pressure Coupling

In our simulations we have controlled the pressure using Berendsen pressure coupling (11) for equilibration MD simulations and by Parinello-Rahman pressure coupling (14,15) in the production MD simulations. In our membrane simulations, we have used semi-isotropic pressure coupling to maintain zero surface tension of the membrane.

2.1.3.1 Berendsen pressure coupling

Similarly to Berendsen temperature coupling, deviations of pressure from the set values are corrected according to the following equation:

$$\frac{dP}{dt} = \frac{P_0 - P}{\tau_p} \tag{2.13}$$

This is accomplished by rescaling the particle coordinates and box vectors every n_{PC} steps with a scaling a matrix μ given by:

$$\mu_{ij} = \delta_{ij} - \frac{n_{PC}\Delta t}{3\tau_p}\beta_{ij}\left\{P_{0ij} - P_{ij}(t)\right\} \tag{2.14}$$

Here P_{oij} and P_{ij} are elements of reference pressure matrix P_0 and instantaneous pressure matrix P, respectively. This algorithm is used in our equilibration simulations. This strong coupling scheme does not simulate true constant pressure ensembles but is efficient at bringing our system to the given pressure.

2.1.3.2 Parrinello Rahman pressure coupling

We have used Parrinello Rahman pressure coupling in the production MD simulations. This method is similar to Nose-Hoover temperature coupling and in theory yields true constant pressure ensemble.

In this algorithm, evolution of the box size obeys the following

$$\frac{d^2 b}{dt^2} = VW^{-1} b'^{-1} (P - P_0) \tag{2.15}$$

Here b is a matrix containing the box vectors (i.e. vectors defining the size and shape of the simulation box), *V* is the volume of the box, *W* is a matrix determining the coupling strength and is given by

$$\left(W^{-1}\right)_{ij} = \frac{4\pi^2 \beta_{ij}}{3\tau_p^2 L} \tag{2.16}$$

Here *L*, is the largest box matrix element

The equations of motion for the particles are

$$\frac{d^2 r_i}{dt^2} = \frac{F_i}{m_i} - M \frac{dr_i}{dt} \tag{2.17}$$

where *M* is the friction coefficient given by

$$M = b^{-1} \left[b \frac{db'}{dt} + \frac{db}{dt} b' \right] b'^{-1} \tag{2.18}$$

2.1.4 Calculation of Instantaneous Temperature and Pressure

Both the temperature and pressure schemes require calculation of instantaneous temperature and pressure. Temperature of an *N* particle system is given by

$$T = \frac{2E_{KE}}{3k_B} = \frac{\sum_{i=1}^{N} m_i v_i^2}{k_B} \tag{2.19}$$

The instantaneous pressure tensor **P** is calculated from the difference in the kinetic energy E_{KE} and the virial Ξ.

$$\mathbf{P} = \frac{2}{V}(E_{KE} - \Xi) \tag{2.20}$$

$$\Xi = -\frac{1}{2}\sum_{i<j} r_{ij} \otimes F_{ij} \tag{2.21}$$

Here r_{ij} is vector connecting the j-th particle with the nearest image of the i-th particle, F_{ij} is the force exerted by the j-th particle on the i-th particle and $\otimes$ represents direct product of two vectors.

2.2 Coarse Grained Molecular Dynamics

Presently, molecular dynamics simulations on the atomic scale are limited to simulation times of less than 1 μs due to the limitations of computer power. One of the possible ways to extend time scales accessible to the molecular dynamics simulations is to use less precise models such as coarse grained molecular dynamic (CGMD) simulations.

The CGMD simulations use “pseudo atoms” to represent group of atoms. This grouping of atoms helps one reduce the number of degrees of freedom and thus extend the time and length-scales accessible to the simulations. For our studies we use the MARTINI CGMD model proposed by Marrink et al(16). The MARTINI CGMD model generally uses 4:1 mapping scheme i.e. on average four heavy atoms are represented as one standard spherical bead. For representation of the underlying atomistic structure, the following four bead types are introduced: C(apolar), P(polar), N(non-polar) and Q(charged). Apart from the 4:1 mapping scheme for standard beads, CGMD also uses 2-3:1 mapping scheme to represent ring compounds. Each bead type has several

subtypes. For example, subtypes of 0, d, a and da indicate hydrogen bonding capabilities: 0(no hydrogen bonding capabilities), d (some hydrogen donor capabilities), a (hydrogen acceptor capabilities) and da (both donor and acceptor capabilities) and subtypes of 1,2,3,4,5 indicate the polarity of the bead: 5 is more than 1.The masses of most beads are set to 72 atomic mass units.

The interactions between the CG beads i and j not connected by a chemical bond are described using the Lennard-Jones(LJ) potential,

$$U_{LJ}(r_{ij}) = 4\varepsilon_{ij}\left[\left(\frac{\sigma_{ij}}{r_{ij}}\right)^{12} - \left(\frac{\sigma_{ij}}{r_{ij}}\right)^{6}\right] \tag{2.22}$$

Here σ_{ij} is the LJ diameter ε_{ij} is the depth of the potential well and i, j represent types of beads. The value of σ_{ij} is 0.47 nm for most of the standard particles. The value ε_{ij} for standard beads is varied from 5.6 KJ/mol for strongly attractive to 2.0 KJ/mol for nearly repulsive interactions. For the interaction between beads representing a ring structure, the value of σ_{ij} is changed to 0.43 nm and the values of ε_{ij} are reduced to 75% of the standard bead values.

The electrostatic interaction energy of N particles and their periodic images is

$$V = \frac{f}{2}\sum_{n_x}\sum_{n_y}\sum_{n_z}{}^{*}\sum_{i}^{N}\sum_{j}^{N}\frac{q_i q_j}{r_{ij,n}} \tag{2.23}$$

Here $f = (4\pi\varepsilon)^{-1}$ and ε is the permittivity of the medium, q_i and q_j are the charges on *i*-th and *j*-th bead respectively, $n = (n_x, n_y, n_z)$ is the index vector of the simulation box, $r_{ij,n}$ is the real distance between the charges, the asterisk indicate that the terms with i=j are omitted when $(n_x, n_y, n_z) = (0,0,0)$

Ewald summation is an elegant method to calculate long range interactions as it converts the single slowly converging sum in Eq.2.23 into two quickly converging terms and a constant term. In this technique, the summation is divided into short range and long range parts which are evaluated in real and reciprocal (Fourier) spaces, respectively.

$$V = V_{dir} + V_{rec} + V_{0,} \tag{2.24}$$

$$V_{dir} = \frac{f}{2}\sum_{i,j}^{N}\sum_{n_x}\sum_{n_y}\sum_{n_z}{}^{*} q_i q_j \frac{erfc(\beta r_{ij,n})}{r_{ij,n}}, \tag{2.25}$$

$$V_{rec} = \frac{f}{2}\sum_{i,j}^{N}\sum_{m_x}\sum_{m_y}\sum_{m_z}{}^{*} \frac{\exp(-(\pi m/\beta)^2 + 2\pi i m(r_i - r_j))}{m^2}, \tag{2.26}$$

$$V_0 = -\frac{f\beta}{\sqrt{\pi}}\sum_{i}^{N} q_i^2, \tag{2.27}$$

The parameter β determines the relative weight of the direct and reciprocal sums. m = (m_x, m_y, m_z). The term V_0 removes the interaction of the particle with itself contained in reciprocal sum.

Small vibrations of the bond length and angles are approximated by harmonic potentials.

$$U_{ijbond}(r) = \frac{1}{2}k_{ij}^{b}(r_{ij} - r_{ij}^{0})^2 \tag{2.28}$$

$$U_{ijkangle}(r) = \frac{1}{2}k_{ijk}^{\theta}(\cos(\theta_{ijk}) - \cos(\theta_{ijk}^{0}))^2 \tag{2.29}$$

Here r_{ij}^{0} and θ_{ijk}^{0} are the equilibrium bond lengths and bond angles and, k_{ij}^{b}, k_{ijk}^{θ} are the force constants. All our simulations were performed using software GROMACS (21).

The CG models and the corresponding atomic structures of the considered species are shown in Figure 2.1. Every four water molecules in the system were modeled as one single P type -bead.

The membrane bilayers are modeled using saturated dipalmitoyl-phosphatidylcholine (diC_{16}-PC) lipids, unsaturated dilinoleyl- phosphatidylcholine (di$C_{18:2}$-PC) lipids and cholesterol. The diC_{16}-PC, di$C_{18:2}$-PC and cholesterol CG models were developed by Marrink et al(17)(18).

The diC_{16}-PC and di$C_{18:2}$-PC lipid molecule consist a hydrophilic head group, an ester backbone, and two hydrophobic tails. The zwitterionic head group of these lipids consists of choline (modeled as Q0 bead with positive charge) and a phosphate group (modeled as Qa bead with negative charge). The ester backbone of lipids is modeled as two Na beads. The two hydrophobic tails are modeled as two chains, each containing four C beads. The only difference between the models of diC_{16}-PC and di$C_{18:2}$-PC is the double bonds in the tails of di$C_{18:2}$-PC.

The polar head group of cholesterol was modeled as a P bead. The sterol body was modeled by using a ring of five C beads. The hydrophobic tail was modeled as a chain of two C beads.

In addition, we introduced several artificial lipids in order to investigate effects of the lipid structure on the raft formation. By replacing zwitterionic head group of diC_{16}-PC with a negatively charged head group we have prepared an artificial lipid which we call as E-type lipid. Specifically, we replaced the positive charge of the Q0 bead by a negative charge of the same magnitude and removed the charge from the Qa bead.

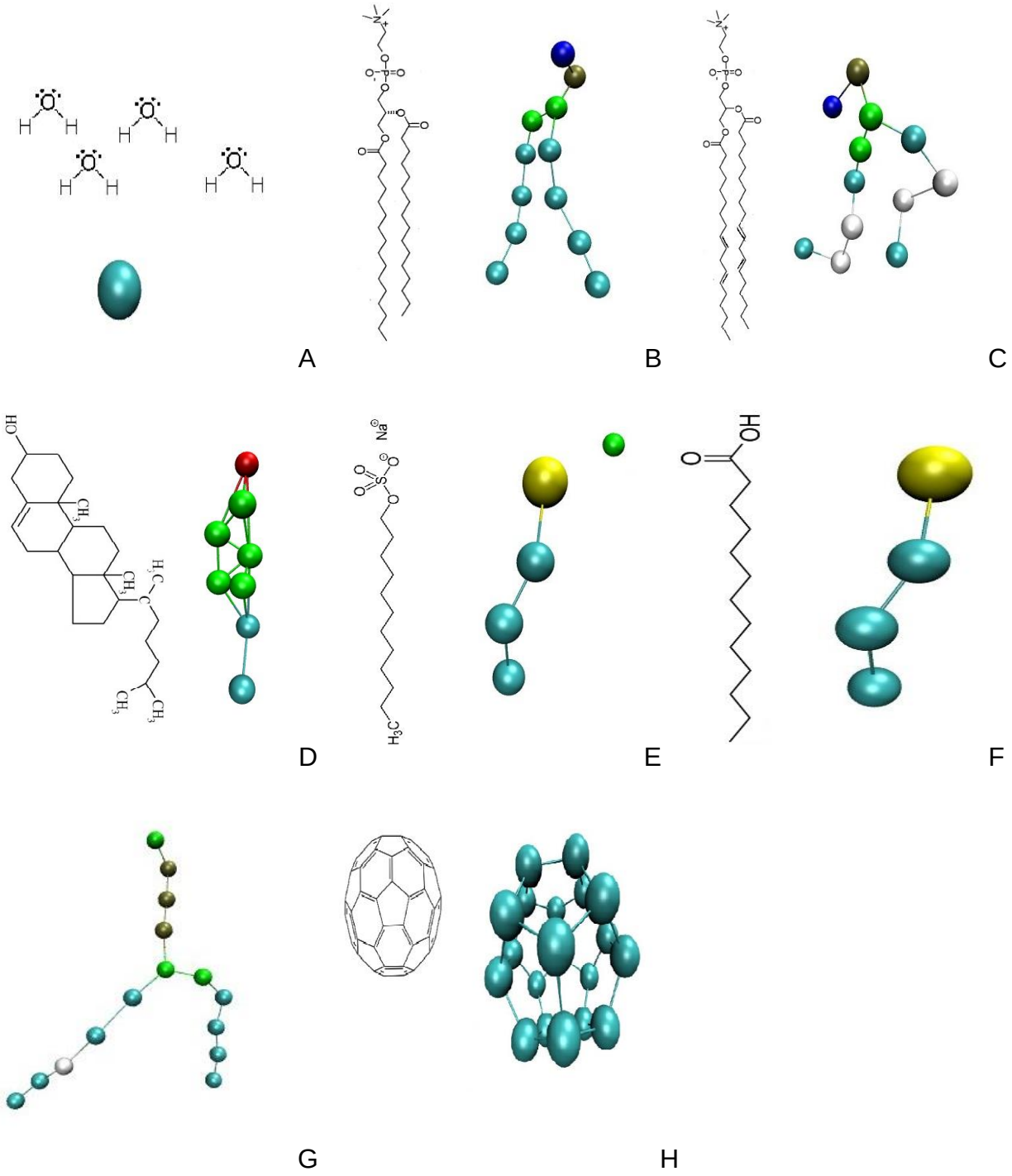

Figure 2-1. Coarse grained models including corresponding atomistic structures of A)Water B) diC_{16}-PC C) di$C_{18:2}$-PC D) cholesterol E) SDS F) Tridecanoic acid G)Q type lipid H)Fullerene nanoparticle

Q type lipids were defined as lipids consisting of hydrophilic head group, an ester backbone and two hydrophobic chains. The head group is composed of a chain of beads containing a polar P4 bead and three charged Qa beads. The ester bone is modeled as two Na beads. The hydrophobic tails are modeled as two chains, with four C beads in one chain and five C beads in other. In addition, we introduced N type lipid which is similar to the Q type lipid and was obtained by replacing the charged Qa beads of the Q-type lipid with Na beads.

In order to investigate effects of electrostatics on the surfactant membrane interactions, Sodium Dodecyl Sulfate (SDS) and Tridecanoic acid were considered. The SDS was modeled using a negatively charged Qa bead for representing sulfate group and three C beads to represent the tail. The Tridecanoic Acid surfactant is similar to SDS; here the charged Qa bead is replaced by a P bead. The motivation for considering these two surfactants was to investigate electrostatic effects of interactions with membrane.

The CG model for fullerene C_{60} was based on the model proposed by D'Rozario et al(19). The C_{60} is modeled by placing 20 evenly spaced C-beads on a sphere of diameter ~1.1nm. A 3:1 mapping is employed here. To preserve the shape of fullerene, the bond lengths and angles between C-beads were constrained.

2.3 Stochastic Model for Nanoparticle Transport

The time scales of transport of molecules and nanoparticles across lipid membrane are too large for direct MD simulations. The transport rates are therefore calculated by using an indirect method known as potential of mean force (PMF) method.

The C_{60} transport across lipid bilayer was assumed to be described by the Langevin equation(20)

$$m\ddot{z}(t) + \gamma(z)\dot{z}(\tau) + \frac{dG(z)}{dz} = \Gamma(z,t) \tag{2.30}$$

Here γ is the friction coefficient, m is mass of particle, G is the free energy, z is the direction of transport, and Γ (z, t) is random force.

In our system, the lipid bilayer is parallel to the xy plane. The distance between the centers of mass of nanoparticle and lipid membranes are constrained at different distances along the z axis by applying constrained force (F). The nanoparticle was free to move in the x and y directions. The average of the constrained force is directly related to PMF.

$$\left\langle F(z_0,t)\right\rangle = \frac{dG(z_0)}{dz} \tag{2.31}$$

CHAPTER 3
RAFT FORMATION

3.1 Stability of Surfactant Aggregates in Lipid Membranes

3.1.1 Background

The surfactants on contact with lipid membrane get adsorbed in the exposed lipid membrane leaflet. This adsorption of surfactant increases the pressure in the leaflet leading to increased permeability (22). This increase in permeability is often transient (7), i.e. the permeability of lipid bilayer eventually decreases. The decrease in permeability is called as healing. A hypothesis for explaining the healing of the bilayer states that healing may be due to jumping of surfactant molecules between the outer and inner layers of the bilayer and/or aggregation of surfactant molecules (8). In this section we present our MD simulations for investigate the possibility of surfactant aggregation in the diC_{16}-PC membrane. To this end, we consider stability of preassembled surfactant aggregates in a bilayer.

3.1.2 Simulation Details

An initial system containing preassembled surfactant aggregate was created. The aggregate was then surrounded by a lipid bilayer. In our system, we have used SDS, Tridecanoic Acid and diC_{16}-PC coarse grained models as described in Section 2.2. Initially, we arranged 628 SDS molecules in a circular bilayer structure to represent an aggregate as shown in Figure 3.1. The aggregate contains equal number of surfactant molecules in each layer.

The distance between the Qa beads of SDS molecules across the bilayer was varied in order to investigate the dependency of aggregate stability on its thickness. Two distances 4.36nm and 2.6nm were considered for this purpose. The distance of

4.36nm was considered for making SDS aggregate thickness nearly equal to that of the diC_{16}-PC bilayer and distance of 2.6nm was considered as it is nearly equal to the diameter of a SDS micelle. The horizontal spacing between SDS molecules was 0.5 nm. This distance is greater than the bead diameter (σ = 0.47nm) and was chosen to avoid an overlap between the molecules. The surfactant aggregate was then surrounded by diC_{16}-PC bilayer, water and sodium ions. All lipid molecules overlapping with the surfactant molecules were removed. We added 628 Na+ ions to neutralize the system.

The resultant system consists of 628 molecules of SDS, 1957 molecules of diC_{16}-PC, 628 Na+ ions and 36294 beads of water in a box with dimensions 27nm x 27nm x 11nm. An energy minimization is performed using the steepest descent algorithm. The system is then equilibrated for 200ns at 323 K temperature and 1 bar pressure, allowing some of the lipids in the bilayer to relax while positions of SDS molecules are restrained. The resultant system is shown in Figure 3.1. The position restraint on the SDS molecules was then removed and a production MD simulation was performed using both long range and short range electrostatics.

In order to understand the contribution of electrostatic interactions for stabilizing our surfactant aggregate, we repeated the simulations for a system in which the anionic SDS surfactants were replaced by neutral Tridecanoic Acid surfactants.

3.1.3 Results

The surfactant aggregates are observed to be unstable. They disperse throughout the lipid bilayer in few nanoseconds of removal of the position restraint. For the short-range electrostatic model, the SDS aggregate with the initial thickness of 4.36 nm dispersed throughout the membrane within 90 ns as shown in Figure 3.2. In the

case of long-range electrostatics, some of the SDS molecules were observed to desorb from the bilayer. This behavior is most probably due to increased attraction of SDS by Na+ ions which pulled them out of the bilayer. The remaining SDS molecules dispersed throughout the bilayer within 80 ns.

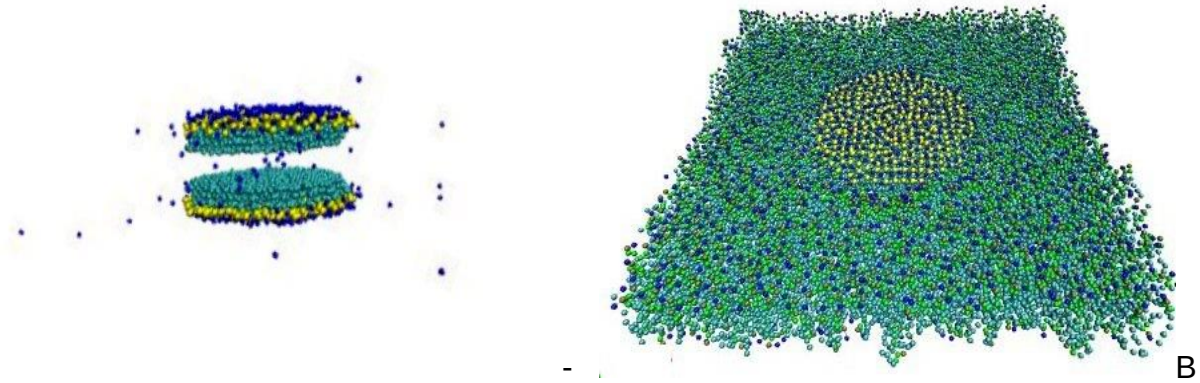

A - B

Figure 3-1. Initial conditions for MD simulations for exploring stability of pre-assembled surfactact aggregate A) Pre assembled SDS aggregate B) diC_{16}-PC lipid bilayer containing a pre-assembled SDS aggregate

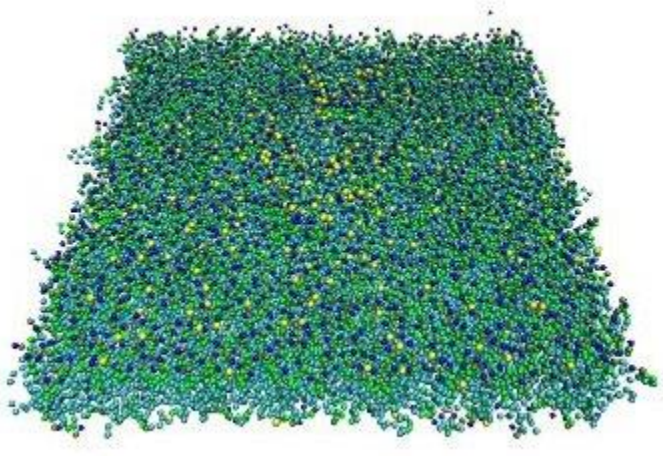

Figure 3-2. Results of MD simulations showing dispersion of SDS aggregate throughout the diC_{16}-PC lipid bilayer

In the simulations with the SDS aggregate of initial thickness of 2.6nm, we observed that the SDS aggregate dispersed in membrane in 85 ns. The Tridecanoic

Acid aggregate with thickness of 4.36nm dispersed throughout the membrane within 70 ns. The difference between these times is too small to perform meaningful comparison between the systems. The dispersion of surfactant molecules in all our simulations suggests that the considered surfactants do not form aggregates in diC_{16}-PC bilayer.

3.2 Phase Separation of Lipids Due to Cross Bridging by Calcium Ions

3.2.1 Background

Lipids in the membranes are known to aggregate into domains of different composition resulting in heterogeneity of the bilayer. Many mechanisms as stated in Chapter 1 are proposed for explaining the aggregation of lipids.

In contrast to our observations reported in the Section 3.1, Pantano et al(23) observed raft formation of surfactant molecules. Their modeled system consists of surfactants which mimic charged and neutral surfactants called C and N-type surfactants, respectively. The C and N-type surfactant is modeled using 5 hydrophilic and 7 hydrophobic beads to represent the hydrophilic and hydrophobic parts of surfactants. In C-type surfactants, three head group beads were modified to mimic charged beads. Cross linker ion like particles which mimic calcium were added to the system. The size of crosslinker ion and its interaction strength with the charged group mimicking beads of the C-type surfactants was varied to drive the segregation. It is important to note that the beads mimicking the charges did not include real charges. The simulations resulted in formation of domains composed of C type surfactants and Calcium ions.

In our study, we are investigating raft formation using artificial lipid molecules which are similar to the surfactant molecules used by Pantano et al. However our study greatly differs from Pantano as in our simulations, we have used explicit charges for

driving the segregation of lipids due to crosslinking by calcium ions which acts as crossbridges. This results in a more realistic representation of electrostatic forces in our system.

3.2.2 Model and Simulation Details

We considered three models systems: a mixture of diC_{16}-PC and Q type lipids, a mixture of Q type lipids and N type lipids and a mixture of diC_{16}-PC and E-type lipid. The models of diC_{16}-PC, Q type, N type and E-type lipids were described in Section 2.2. The system compositions and simulation details are summarized in Table 3-1.

Table 3-1. Details of the systems considered in simulation of aggregate formation due to salt bridges.

System	Composition	Duration of simulation	Box size	Simulation parameters	Initial conditions
System 1	1600 diC_{16}-PC lipids, 1600 E-type lipids, 49200 water beads and 800 Ca2+ ions.	400ns	31nm x 31nm x 10nm	Long-range electrostatics. Temperature =323 K. Pressure =1 bar	Bilayer of diC_{16}-PC lipids and 1600 E-type lipids surrounded by water and calcium ions.
System 2	196 diC_{16}-PC lipids, 196 Q-type lipids, 6174 water beads and 294 Ca^{2+} ions and 6174 beads of water	200ns	11nm x 12nm x 9nm	Long-range electrostatics. Temperature =323 K. Pressure =1 bar	Randomly dispersed lipids and ions in water
System 3	838 molecules of N-type lipid, 246 molecules of Q type lipid, 369 Ca2+ ions and 13924 representing water	200ns	14nm x 14nm x 14nm	Long-range electrostatics. Temperature =323 K. Pressure =1 bar	Lipids are arranged in form of bilayer by placing lipids apart by 0.5nm

A system containing diC_{16}-PC and E-type lipids was considered to analyze if the Ca2+ ions can cross link lipids and drive the aggregation of lipids having only one charged bead in a head group. For creating the initial bilayer system, half of the lipids in a self-assembled diC_{16}-PC bilayer system were replaced by E-type lipids.

Our second system initially contains a random mixture Q type lipids and diC_{16}-PC. A Q-type lipid contains 3 charged beads in head group for driving the aggregation by electrostatic coupling with Ca2+ ions.

In our third system, we created a bilayer containing Q-type and N-type lipids. These lipids contain equal number of beads for representing the head and tail groups. This system was considered to explore the influence of headgroup length of neutral lipids on the aggregation.

3.2.3 Results

No segregation of lipids has occurred in the System 1. The random initial mixtures of Systems 2 and 3 self-assembled into worm-like micelles and bilayer like structures shown in Figure 3.3 and 3.4, respectively. We note that an equilibrium self-assembled structure in System 3 is likely to be a bilayer. The defects of the bilayer-like structures formed in our simulation are likely due to a large size of the simulation box. It is likely that a perfect bilayer can be obtained by performing self-assembly simulations in a system of a smaller size or by simulating the system for a very long period of time.

The high number of Ca2+ ions near the head groups of Q-type lipids suggests that lipid segregation takes place due to the crosslinking of Q-type lipids by Ca2+ ions. This segregation of Q type lipid molecules is in agreement with the study of Pantono el at. However the segregation of the lipids was not observed when the lipids have only

single charged head groups indicating that the aggregation occurs only for lipids with several charged groups in their head groups.

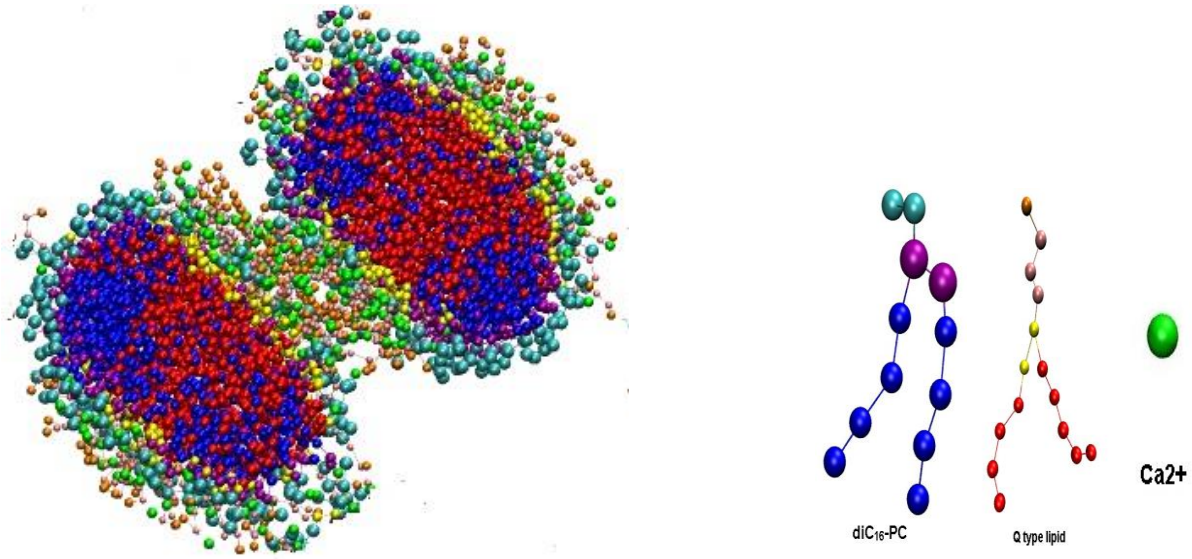

Figure 3-3 .Worm like micelles with aggregation of Q type lipids

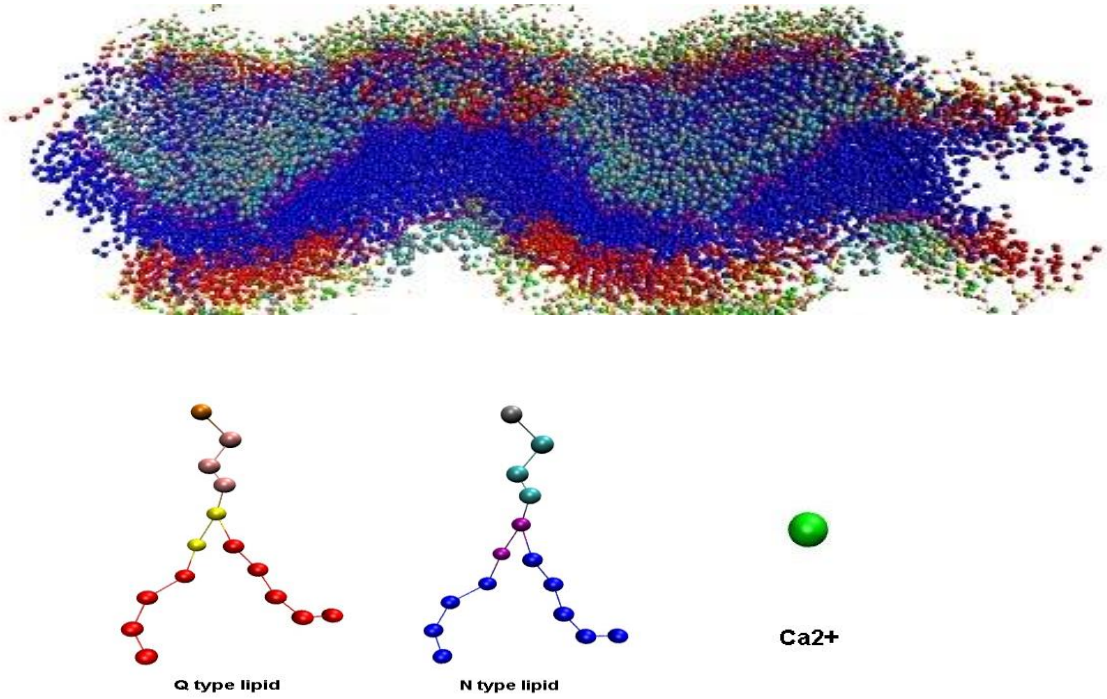

Figure 3-4 . Bilayer system containing Q-type and N-type lipids. Note: The Q type lipid aggregation can be observed.

3.3 Phase Segregations in Tertiary Lipid Mixtures : Effect of Cholesterol

3.3.1 Background

In the Section 3.2, we have considered the aggregation of artificial lipids due to crosslinking by ions. Here, we turn to a widely known natural lipid segregation mechanism which occurs due to the presence of cholesterol.

The biological membranes separate in to various domains including the liquid ordered (L_o) and liquid disordered (L_d) phases. This segregation takes place in the presence of cholesterol at biologically relevant concentrations (10-30%). The L_o phase is enriched with cholesterol and saturated lipids and the L_d phase is mostly composed of unsaturated lipids.

Lipid bilayers generally exist as either disordered liquid crystalline or ordered gel phases. The liquid ordered phase L_o is perceived as an intermediate phase between the liquid crystalline and gel phases. Many theories are proposed to explain formation of the L_o phases. One of the hypotheses is that cholesterol interacting with saturated lipids increases the degree of orientation order of membrane leading to a tighter packing. This hypothesis was confirmed by simulations of Risselada el at(24) .The goal of the current study is to understand the segregation and prepare samples of different membrane phases to be used in analysis of transport of fullerene across these phases.

3.3.2 Model and Simulation Details

In this system the saturated and unsaturated lipids in a biomembrane were modeled using diC_{16}-PC and di$C_{18:2}$-PC respectively. According to the simulations carried by Risselada el at(24), an initial system of diC_{16}-PC/di$C_{18:2}$-PC/cholesterol molecules in the ratio of 0.48:0.28:0.3 have separated in to two equilibrium phases.

These phases were called Lo and Ld phase with compositions of diC_{16}-PC/$diC_{18:2}$-PC/cholesterol in the ratio 0.61:0.01:0.37 and 0.08:0.75:0.17, respectively.

A bilayer structure was obtained by Risselada el at(24) and posted in website(25). The system consists of 828 diC_{16}-PC molecules, 540 $diC_{18:2}$-PC molecules, 576 cholesterol molecules and 12600 water beads. To this system, 45345 additional water beads were added and the resulting box size was 22nm x 22nm x 18nm. MD simulation is performed for 200ns at a temperature of 323K to melt the ordered phase. This is followed by an MD simulation for 1000ns at 295K.

A 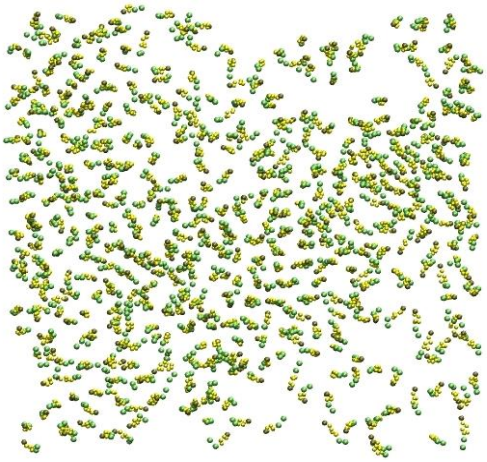 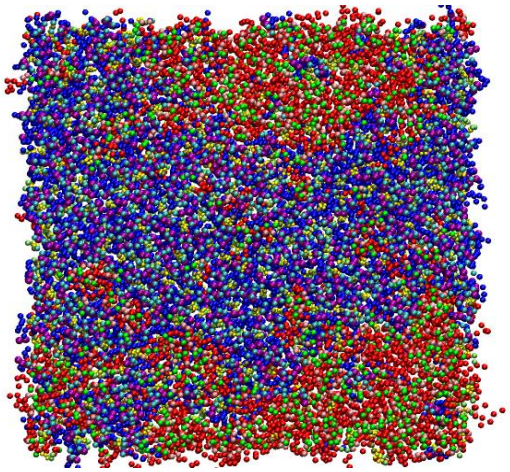 B

C 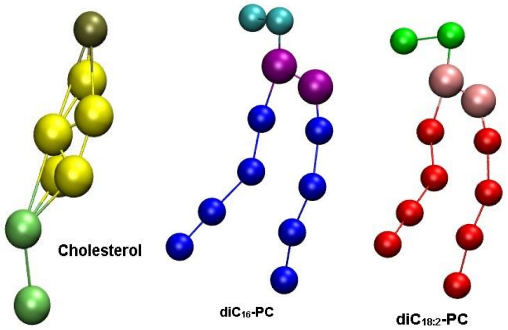

Figure 3-5 Distribution of components of bilayer at 323K A) The cholesterol distribution in the bilayer at 323K B) The corresponding distribution of lipids in the bilayer. C) The Color coding of cholesterol and lipids

3.3.3 Observations

At 323K, the ordered phase melted dissolving the phase boundary as shown in Figure.3.5. The system shown in Figure 3.5 did not reach the steady state. The lipids are expected to mix completely and result in a homogeneous phase upon simulating the system for a longer period of time at 323K. Reducing the temperature of the system to 295 K leads to phase separation as shown in Figure 3.6. The figures show that the degree of separation in the ternary mixtures of diC_{16}-PC, di$C_{18:2}$-PC and cholesterol is temperature dependent.

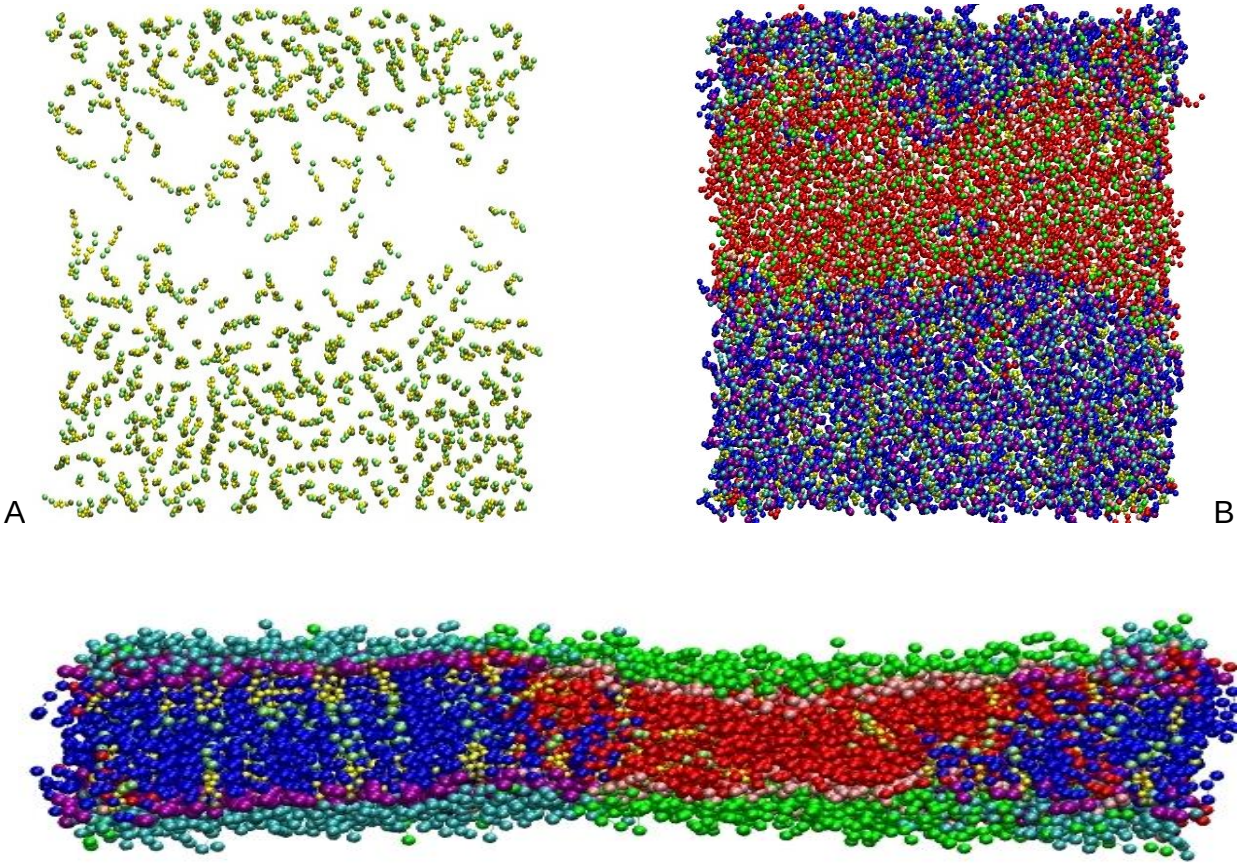

A B

C

Figure 3-6 Distribution of components of bilayer at 295K A) The cholesterol distribution in the bilayer B) The corresponding distribution of lipids in the bilayer. C) The Cross sectional view of the bilayer. Note that the cholesterol has shown preference towards the diC_{16}-PC molecules.

In the Chapter 4 we investigate nanoparticle transport across the L_o and L_d phases are modeled as a ternary mixture of diC_{16}-PC, di$C_{18:2}$-PC and cholesterol. On the basis the composition obtained by Risselada el at(24) for L_o and L_d phases, we have prepared two bilayer systems. The bilayer system with 264 diC_{16}-PC molecules, 5 di$C_{18:2}$-PC molecules, 160 cholesterol molecules and 10586 beads of water is prepared to represent L_o phase. Our L_d phase is represented by a bilayer containing 264 di$C_{18:2}$-PC molecules, 60 cholesterol molecules, 28 diC_{16}-PC molecules and 10586 beads of water.

CHAPTER 4
TRANSPORT OF FULLERENE NANOPARTICLE INTO LIPID MEMBRANE

4.1 Background

Understanding permeation of nanoparticles into the cell membrane has great importance in nanotoxicology research. In our work we have focused on a transport of a hydrophobic fullerene nanoparticle across the membrane. The fullerene nanoparticles are composed of carbon atoms hold promise in the areas of drug delivery, antimicrobial therapy (26), diagnostic imaging and cancer research (27). However, both the pristine and functionalized fullerenes have been shown to exhibit toxicity (28). One of the possible toxicity mechanisms is generation of reactive oxygen species (ROS) causing lipid peroxidation and cell death (29). Besides this mechanism nanoparticles can also damage the integrity of membranes by physical mechanisms. Most of earlier molecular dynamics studies of the transport of fullerene nanoparticles into the lipid membranes have been performed for single component lipid membranes (19,30,31). These studies have shown that fullerenes can enter the lipid membrane with ease and stay in the membrane for a very long time. It is thus possible that this long residence of nanoparticles in membranes leads to membrane destabilization.

The goal of Chapter 4 is to explore effect of the membrane composition on nanoparticle transport across membranes. Specifically, we analyzed the transport of fullerene across the liquid-ordered and liquid-disordered phases of membranes composed of saturated and unsaturated lipids and cholesterol.

4.2 Model and Simulation Details

The models of the liquid ordered (Lo) and liquid disordered (Ld) phases of a lipid bilayer were created using diC_{16}-PC, di$C_{18:2}$-PC and cholesterol as described in Section 2.2.

The two bilayer systems were equilibrated for 200ns at a temperature of 295 K and pressure of 1 bar. A model C_{60} was then introduced into the systems. An energy minimization simulation is preformed followed by a MD equilibration simulation of the system for 100ns.

The free energy profiles for the transport of the model fullerene nanoparticle across the L_o and L_d lipid phases are obtained using the constrained simulations described in Section 2.3. In this method we constrain the distance between the center of masses of C_{60} and lipid bilayer at different positions along the z-direction (recall that the bilayer is parallel is parallel to the x-y plane). The initial conditions for the constrained simulations were obtained by application of an artificial force to pull C_{60} through a bilayer at a rate of 0.0001 nm/ps. The pulling simulations yielded systems with distances between the centers of mass of C_{60} and membrane varying from 0.2 nm to 6 nm. Constraining the distance between the centers of mass, we performed production MD simulations for 400ns using the time step of 0.01 ps to obtain the free energy profile.

4.3 Results

The obtained free energy profiles for the transport of C60 into the membrane phases are shown in the Figure 4.1.

The free energy profiles for the fullerene nanoparticle transport across the L_o and L_d phases show a great qualitative difference. The profiles indicate that in both phases the fullerene present in water is attracted towards the bilayer center. This is due to hydrophobic attraction between the hydrophobic fullerene and hydrophobic tails of the lipids.

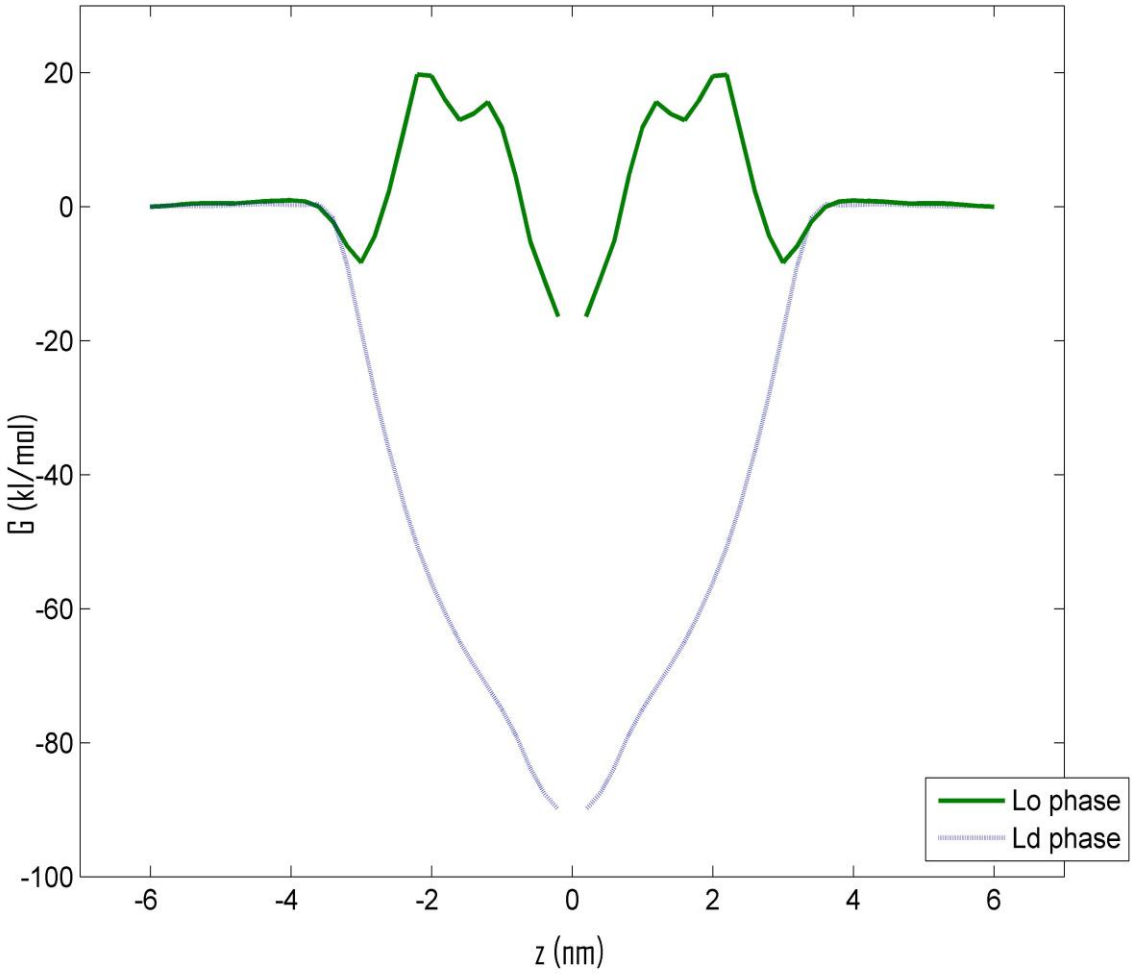

Figure 4-1. Free energy profiles for the transport of the model fullerene nanoparticle across the L_o and L_d lipid phases

In L_d phase, the fullerene is shown to easily enter the bilayer with negligible resistance. The hydrophilic head groups of the lipids do not provide any observable resistance to the transport. This is due to the similarity between interactions of fullerene with hydrophilic head groups and water. Upon entering the membrane, fullerene continues to experience hydrophobic attractions which move it to the center of the membrane. The energy profile for the Ld phase is similar to the previous simulations studies (19,30,31) and indicates that the fullerene can easily enter the membrane.

On the other hand, in the L_o phase the fullerene experiences a high energy barrier of height ~20 KJ/mol at the entrance. This energy barrier is likely due to the tight packing of the lipids and cholesterol in the Lo phase. Upon the entry of nanoparticle into the bilayer, the free energy increases gradually which is likely due to the increase in density of cholesterol rings. The free energy profile then decreases as the fullerene moves towards the center of the bilayer due to the hydrophobic attraction by tail groups and also due to a decreased thickness of the cholesterol rings.

The computed free energy profiles indicate that the C60 nanoparticles are more likely to be present in the L_d phase of the membrane as the L_o phase provides a larger resistance to their entry.

LIST OF REFERENCES

1. May, S. 2009. Trans-monolayer coupling of fluid domains in lipid bilayers. Soft Matter 5, 3148-3156

2. Collins, M. D. 2008. Interleaflet coupling mechanisms in bilayers of lipids and cholesterol. Biophys. J. 94, L32-L34.

3. McMullen, T., R. Lewis and R. McElhaney 2004. Cholesterol-phospholipid interactions, the liquid-ordered phase and lipid rafts in model and biological membranes. Curr. Opin. Colloid Interface Sci. 8, 459-468.

4. Leibler, S. and D. Andelman 1987. Ordered and curved meso-structures in membranes and amphiphilic films. Journal De Physique. 48, 2013-2018.

5. Xia, W. and H. Onyuksel 2000. Mechanistic studies on surfactant-induced membrane permeability enhancement. Pharm. Res. 17, 612-618.

6. Groot, R. and K. Rabone 2001. Mesoscopic simulation of cell membrane damage, morphology change and rupture by nonionic surfactants. Biophys. J. 81, 725-736.

7. Lesieur, S., C. Grabielle-Madelmont, C. Menager, V. Cabuil, D. Dadhi, P. Pierrot and K. Edwards 2003. Evidence of surfactant-induced formation of transient pores in lipid bilayers by using magnetic-fluid-loaded liposomes. J. Am. Chem. Soc. 125, 5266-5267

8. Gupta, C., A.K. Daechsel and A. Chauhan 2011. Interaction of ionic surfactants with cornea-mimicking anionic liposomes. Langmuir. 27, 10840-10846.

9. The Woodrow Wilson Center's Project on Emerging Nanotechnologies (PEN) news 2011. http://www.nanotechproject.org/news/archive/9231. Accessed 2013 FEB

10. Verlet, L. 1967. Computer experiments on classical fluids .I. thermodynamical properties of lennard-jones molecules. Physical Review. 159, 98-&.

11. Berendsen, H., J. Postma, W. Vangunsteren, A. Dinola and J. Haak 1984. Molecular-dynamics with coupling to an external bath. J. Chem. Phys. 81, 3684-3690.

12. Nose, S. 1984. A molecular-dynamics method for simulations in the canonical ensemble. Mol. Phys. 52, 255-268.

13. Hoover, W. 1985. Canonical dynamics - equilibrium phase-space distributions. Phys. Rev. A. 31, 1695-1697

14. Parrinello, M. and A. Rahman 1981. Polymorphic transitions in single-crystals - a new molecular-dynamics method. J. Appl. Phys. 52, 7182-7190.

15. Nose, S. and M. Klein 1983. Constant pressure molecular-dynamics for molecular-systems. Mol. Phys. 50, 1055-1076

16. Marrink, S. J., H.J. Risselada, S. Yefimov, D.P. Tieleman and A.H. de Vries 2007. The MARTINI force field: Coarse grained model for biomolecular simulations. J Phys Chem B. 111, 7812-7824

17. Marrink, S. J., A.H. de Vries, T.A. Harroun, J. Katsaras and S.R. Wassall 2008. Cholesterol shows preference for the interior of polyunsaturated lipid. J. Am. Chem. Soc. 130, 10-+.

18. Marrink, S., A. de Vries and A. Mark 2004. Coarse grained model for semiquantitative lipid simulations. J Phys Chem B. 108, 750-760.

19. D'Rozario, R. S. G., C.L. Wee, E.J. Wallace and M.S.P. Sansom 2009. The interaction of C-60 and its derivatives with a lipid bilayer via molecular dynamics simulations. Nanotechnology. 20, 115102.

20. Gardiner, C. W. 2004 Handbook of Stochastic Methods for Physics, Chemistry and the Natural Sciences. 3rd Ed Springer.

21. Van der Spoel, D., E. Lindahl, B. Hess, G. Groenhof, A. Mark and H. Berendsen 2005. GROMACS: Fast, flexible, and free. J. Comput. Chem. 26, 1701-1718.

22. Heerklotz, H. and J. Seelig 2007. Leakage and lysis of lipid membranes induced by the lipopeptide surfactin. Eur. Biophys. J. Biophys. Lett. 36, 305-314.

23. Pantano, D. A., P.B. Moore, M.L. Klein and D.E. Discher 2011.
Raft registration across bilayers in a molecularly detailed model. Soft Matter. 7, 8182-8191.

24. Risselada, H. J. and S.J. Marrink 2008. The molecular face of lipid rafts in model membranes. Proc. Natl. Acad. Sci. U. S. A. 105, 17367-17372.

25. Risselada, H. J. and S.J. Marrink 2008. The molecular face of lipid rafts in model membranes http://md.chem.rug.nl/cgmartini/images/applications/bichol/raft.gro Last accessed , 2013 JAN

26. Tegos, G., T. Demidova, D. Arcila-Lopez, H. Lee, T. Wharton, H. Gali and M. Hamblin 2005. Cationic fullerenes are effective and selective antimicrobial photosensitizers. Chem. Biol. 12, 1127-1135.

27. Chen, Z., R. Mao and Y. Liu 2012. Fullerenes for cancer diagnosis and therapy: Preparation, biological and clinical perspectives. Curr. Drug Metab. 13, 1035-1045

28. Oberdorster, E. 2004. Manufactured nanomaterials (fullerenes, C-60) induce oxidative stress in the brain of juvenile largemouth bass. Environ. Health Perspect. 112, 1058-1062.

29. Trpkovic, A., B. Todorovic-Markovic and V. Trajkovic 2012. Toxicity of pristine versus functionalized fullerenes: Mechanisms of cell damage and the role of oxidative stress. Arch. Toxicol. 86, 1809-1827.

30. Kopelevich, D. I., J. Bonzongo, R. A. Tasseff, J. Gao, Y. Ban and G. Bitton.2008; 2008.Potential toxicity of fullerenes and molecular modeling of their transport across lipid membranes; In Nanoscience and nanotechnology, John Wiley & Sons, Inc., 233-260.

31.Baowan, D., B.J. Cox and J.M. Hill 2012. Instability of C-60 fullerene interacting with lipid bilayer. J. Mol. Model. 18, 549-557.

BIOGRAPHICAL SKETCH

Tarun Narra received a Bachelor of Technology degree in Chemical Engineering from Osmania University, Hyderabad, India in 2011. He received his Master of Science degree in chemical engineering from University of Florida in May 2013. During his masters, he worked under the supervision of Prof. Dmitry I Kopelevich.